

# Gold Nanoparticle Translocation Across a Droplet Interface Bilayer via Dark-Field Microscopy

Jean-Baptiste Fleury,<sup>\*,†</sup> Sean Moro,<sup>‡</sup> Virginie Faure,<sup>‡</sup> and Xavier Le Guével<sup>‡</sup>

<sup>†</sup>*Universität des Saarlandes, Experimental Physics and Center for Biophysics, 66123 Saarbruecken, Germany*

<sup>‡</sup>*University of Grenoble Alpes, Institute for Advanced Biosciences (IAB) - INSERM U1209 - CNRS UMR 5309- 38000 Grenoble, France*

E-mail: jean-baptiste.fleury@physik.uni-saarland.de

## Abstract

For a wide range of biomedical applications, measuring the transport of metal nanoparticles across a cell membrane is of tremendous interest. Such studies are gaining high importance due to applications, especially in the field of drug delivery using NPs. In this work, we measure the passive transport of arginine-functionalized ultra-small gold nanoparticles (AuNPs) with sizes lower than 3 nm across a planar lipid bilayer formed with the droplet interface bilayer (DiB) technique. The AuNPs transport is monitored using dark-field microscopy, which enables the tracking of AuNPs without the use of fluorescent labeling. The measurements of high numbers of events provide a robust quantitative estimation of AuNP translocation dynamics and energy barrier obtained from the lipid bilayer translocation analysis. Interestingly, we observed that the arginine number coated onto AuNP and the bilayer packing control the AuNPs translocation across the lipid bilayer.

# Introduction

The translocation of biologically active particles through cell membranes is of vital importance for cells and is a key process for drug delivery.<sup>1,2</sup> The drug's ability to cross a membrane is largely dependent on the physicochemical properties of the drug.<sup>3</sup> Thus, there is a high interest to develop simple techniques and methods to evaluate quickly and accurately the physical parameters driving delivery systems to translocate through membranes. Droplet interface bilayers (DIBs) provide an interesting platform for recreating simple cellular phenomena associated with exchange across the membranous barriers, for the prediction of in vivo drug movement, and for their use as scaffolds for electrophysiological measurements.<sup>4</sup> This approach involves dispensing aqueous droplets in an oil bath containing a mixture of lipid molecules.<sup>4</sup> The lipid molecules surround the aqueous droplets, with the headgroup in contact with the droplet and the tail remaining in the oil. When two lipid monolayer-coated droplets are brought into contact, they form a lipid bilayer at their interface.<sup>4,5</sup> DIBs can be combined with the dark-field microscopy imaging technique, which is an effective tool for tracking drugs, macromolecules, or nanoparticles with great potential for fast, effective, cheap, and non-destructive imaging of nanoobjects as long as they act as light scattering probes.<sup>6-8</sup>

As an example, metallic nanoparticles were developed for drug delivery purposes. Gold nanoparticles (AuNPs) are widely used in biomedical applications for therapy and diagnostic and are suitable delivery systems as they can be easily tailored by controlling their size, geometry, and surface chemistry.<sup>1,2,9-11</sup> These systems must have a high colloidal stability in physiological environment, antifouling properties to escape the immune system, the capacity to diffuse to the targeted area and to internalize into cells.<sup>12</sup> In this study, we focus our interest on ultra-small AuNPs (1-10nm) because they have recently shown great potential as effective and safe in vivo biosensors, siRNA delivery systems, or therapeutic agents for the treatment of inflammatory diseases and cancers.<sup>13-17</sup> In addition, AuNPs can be detected by dark-field microscopy without any

fixation or staining using fluorescently labeled nanoparticles.

The cellular internalization pathway of AuNPs depends mainly on the size and surface properties of the employed nanoparticles.<sup>18</sup> In a simplistic manner, large AuNPs (10-100 nm) can penetrate living cells via active processes such as clathrin-mediated endocytosis.<sup>18-20</sup> This mechanism is slow, with a characteristic time on the order of seconds to minutes.<sup>21</sup> It has been reported that small to ultra-small AuNPs (1-10 nm) can penetrate living cells via passive pathway such as diffusion.<sup>18,22</sup> This process is energy-independent and usually takes only hundreds of nanoseconds.<sup>23</sup> The case of passive translocation for ultra-small AuNPs have been extensively studied experimentally and theoretically.<sup>22,24-27</sup> These studies highlight numerous potential pathways through which AuNP can cross a lipid bilayer (as a model cell membrane).<sup>22,24-27</sup> These pathways can be divided into destructive and non-destructive families. In a simple way, NPs that cross a bilayer by going through destructive pathways create an irreversible lipid nanopore inside the bilayer, which causes the bilayer to rupture.<sup>28</sup> In contrast, NPs traveling through a bilayer via non-destructive pathways are producing a reversible lipid nanopore inside the bilayer, or no pore at all.<sup>24,27-29</sup> Su *et al.* observed a window of translocation with a sharp maximum for nanoparticles with a balanced hydrophobicity between hydrophilic and hydrophobic properties as a non-destructive pathway,<sup>30</sup> which seems to be confirmed experimentally by the case of stripped nanoparticles made of domains with hydrophobic and hydrophilic ligands.<sup>29,31</sup> In contrast, in destructive pathways, AuNP are transported via pore formation using, for example, superhydrophobic or hydrophilic AuNPs.<sup>32,33</sup> Despite these efforts, observing the kinetics of such translocations experimentally remains difficult because the translocation of ultra-small particles is an extremely fast process. Thus, it is nearly only possible to measure their translocation dynamics when restricting the experimental observation to the motion of individual fluorescent nanoparticles.<sup>32</sup> However, fluorescent labeling has some drawbacks because it changes the surface properties of nanoparticles, which can change/disturb their properties and their translocation pathways.<sup>29,31-33</sup> In this work, we use dark-field microscopy to measure and compare the

collective translocation of ultra-small AuNPs (1-10nm) with different physical characteristics across a droplet interface lipid bilayer. We demonstrated that this system enables us to measure the AuNP permeability coefficient and to estimate the associated activation energy barrier with success. Moreover, this method is simple, cost-effective, and avoids the need to label the AuNPs with fluorescent molecules.

## Results and Discussion

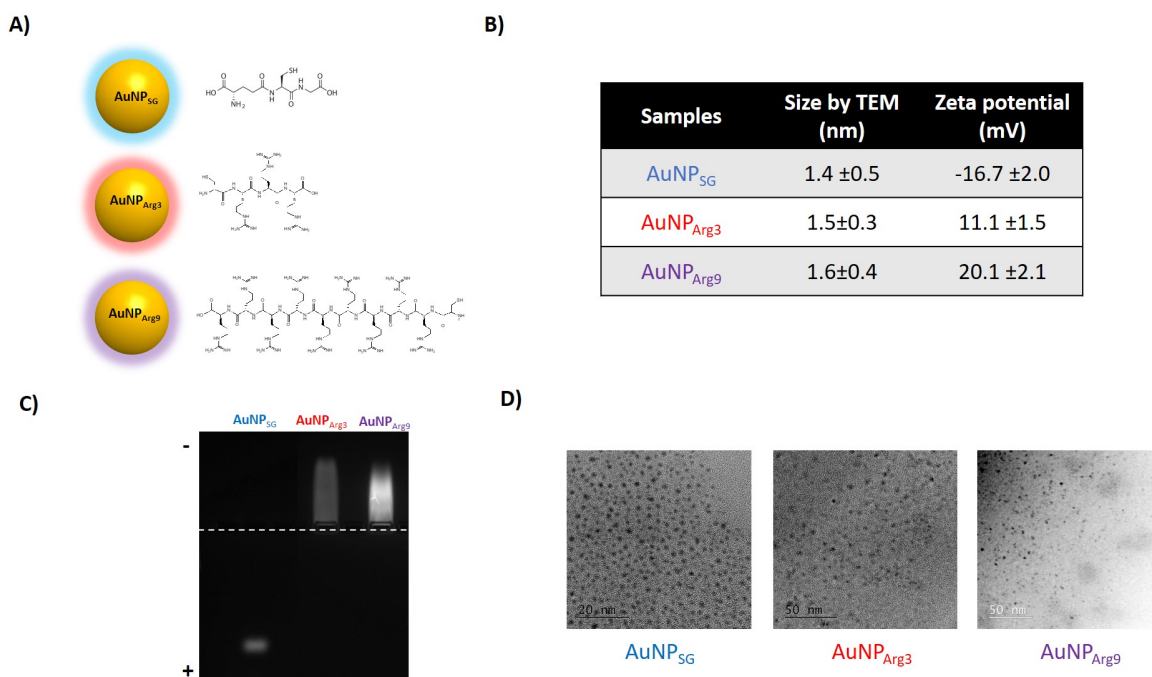


Figure 1: A) Schematic representation of the produced nanoparticles. B) NP size determined by electron transmission microscopy (average of 100 particles) and zeta potential of AuNPs samples in water. C) Agarose gel of AuNPs, AuNP<sub>SG</sub>, AuNP<sub>ARG3</sub>, AuNP<sub>ARG9</sub>. D) TEM micrographs of Au NPs showing particle size smaller than 2 nm.

Ultra-small AuNPs were prepared by a bottom-up approach using the tripeptide Glutathione (SG) for the negatively charged NPs and the incrementally positively charged ligands Arg3 and Arg9, containing 3 and 9 arginines, respectively, to prepare

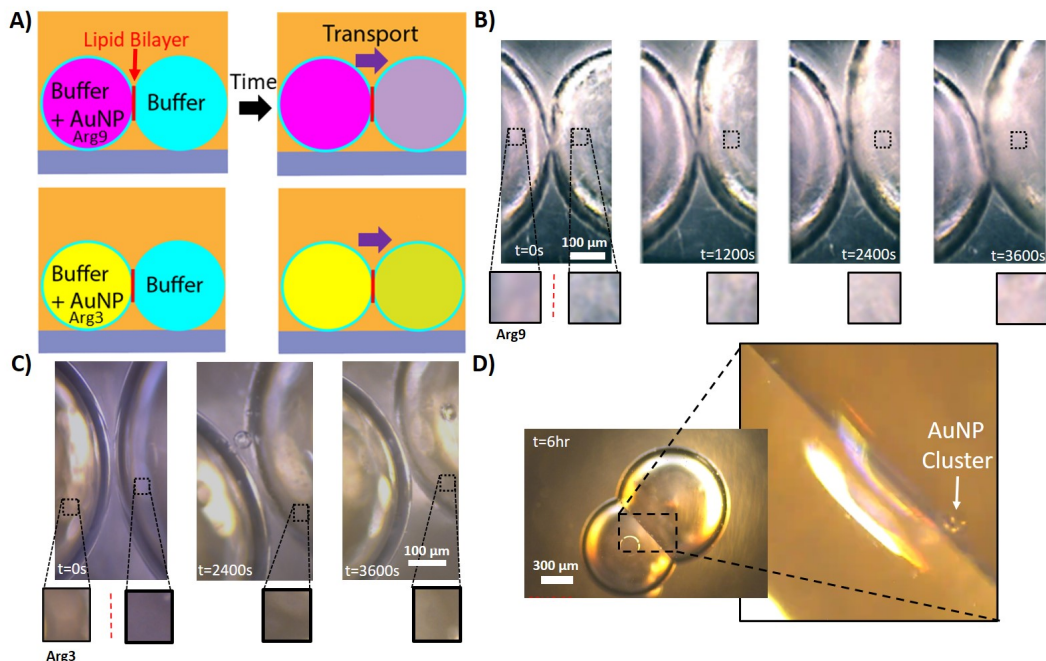


Figure 2: Charge-dependent translocation of AuNP through DiB (video S1) A) Schematic representation of (asymmetric DiB) in a microfluidic chamber micrograph of two buffer droplets in contact with an oily phase containing phospholipids. Series of micrograph of a single DiB system viewed via dark-field microscopy at different time point with left droplet containing 0.2 mg/ml of B)  $\text{AuNP}_{\text{Arg9}}$  (pink color) or C)  $\text{AuNP}_{\text{Arg3}}$  (yellow color) at start. The color change in the second droplet is illustrated in the insets (lower row).D) DiB at 6 hours with the detection of  $\text{AuNP}_{\text{Arg9}}$  clusters at higher magnification (X20).

AuNPs with a tunable positively charged surface (Figure 1). Thanks to the photoluminescence signal of these NPs in the red-near-infrared region, we could see them in agarose gel, due to the negative surface charge for AuNPSG and positive charges for AuNPs containing arginine moiety.<sup>34</sup> Zeta potential measurements of the samples in water confirmed the negative surface for  $\text{AuNP}_{\text{SG}}$  ( $-16.7 \pm 2.0$  mV) and the increased positive surface charge with the amount of arginine in the order  $\text{AuNP}_{\text{Arg3}}$  ( $+11.1 \pm 1.5$  mV), and  $\text{AuNP}_{\text{Arg9}}$  ( $+20.1 \pm 2.1$  mV). TEM measurements showed a relatively good monodispersity ( $CV < 10\%$ ) of NPs with an average size of 1.5 nm (see Figure 1.A). No aggregation of the different AuNPs have been observed over 2 weeks where experiments were conducted on the artificial lipid bilayers. TEM measurements showed a relatively good monodispersity ( $CV < 10\%$ ) of NPs with an average size of 1.5 nm (see Figure 1.D). No aggregation of the different AuNPs have been observed over 2 weeks where

experiments were conducted on the artificial lipid bilayers.

We made a droplet interface bilayer (DiB) in a microfluidic chamber (see Figure 2.A) .<sup>4,5,35</sup> Where one droplet contains only a buffer solution, while the other droplet contains 0.2 mg/ml of AuNPs. Since the start of the experiment, it appears that the droplet containing the AuNPs has a different color than the droplet that does not contain any AuNPs. Also, individual AuNPs (or clusters) can also be seen inside the droplet that contains them (Figure 2.C). Interestingly, after approximately 1 hour, the color signal has become relatively uniform between the droplets, and individual AuNPs can be seen in each droplet (see Figure 2.D and video S1). By doing a color thresholding on the recorded movie (using ImageJ), we can measure the rise of the color signal inside the acceptor droplet. This enables us to calculate the AuNPs transport rate as a function of time. AuNP<sub>Arg9</sub> show a slight pink color and a yellowish color of AuNP<sub>Arg3</sub> by dark field microscopy probably because of the different rate of aggregation on the surface membrane.<sup>36</sup>

We can estimate the passive transport of AuNPs through the bilayer using Fick's law.<sup>35,37-39</sup> Thus, the change in AuNPs through a passive membrane can be calculated as

$$c(t) = \frac{1}{2}c_0e^{-\mu t} + B, \quad (1)$$

where  $c_0$  is the initial AuNPs concentration in the donor droplet,  $\mu$  is the transport rate, and  $B$  is a constant. As a result, we can calculate the color signal intensity as

$$I(t) \approx \frac{1}{2}I_0e^{-\mu t} + C, \quad (2)$$

where  $I_0$  is the initial color signal in the donor droplet and  $C$  is a constant. The measured colored signal in the acceptor droplet as a function of time  $t$ , reveals the intensity increase that is exponential with time. A fit yields the permeability coefficient  $P$  by directly extracting the transport rate  $\mu$ . The transport rate can be used to calculate  $P$ , with

$$P = \mu V_a V_d / ((V_a + V_d) \cdot A). \quad (3)$$

Here,  $V_a$  is the volume of the acceptor droplet,  $V_d$  is the volume of the donor droplet and  $A$  is the bilayer area.

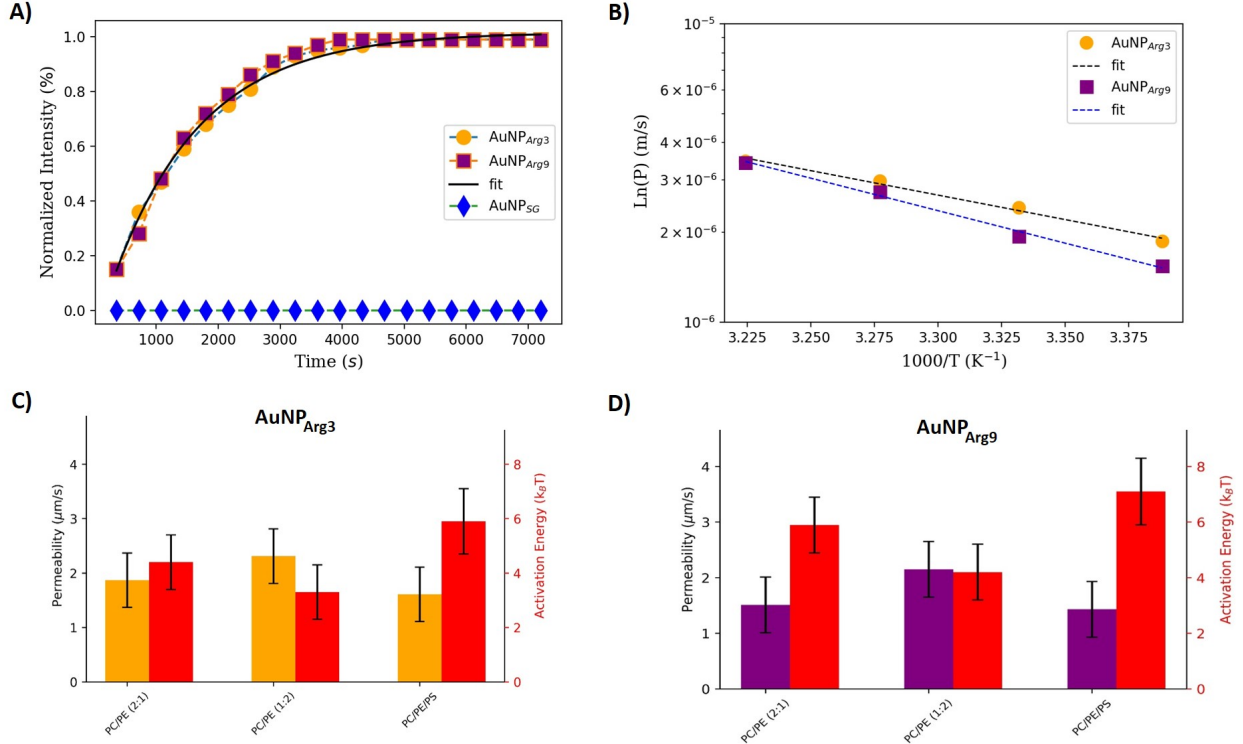


Figure 3: A) Normalized color intensity as a function of time for AuNP<sub>ARG3</sub> and AuNP<sub>ARG9</sub> (with a DOPC/DOPE bilayer in a 2:1 molar ratio). The continuous line is the fit performed with the equation 1. B) Arrhenius plot of the natural log of the permeability coefficient ( $P$ ) versus the reciprocal of the absolute temperature of membranes (same lipidic composition as in A). C-D) Permeability  $P$  and the associated activation energy  $E$  as functions of different lipid bilayer compositions for AuNP<sub>ARG3</sub> and AuNP<sub>ARG9</sub>.

In this experiment, AuNPs with three arginines (AuNP<sub>Arg3</sub>) and AuNPs with nine arginines (AuNP<sub>Arg9</sub>) were used.<sup>40,41</sup> We measured a permeability constant  $P \approx 1.9 \mu m/s$  for AuNP<sub>Arg3</sub> and  $P \approx 1.5 \mu m/s$  for AuNP<sub>Arg9</sub>. These numbers are in the same order as some translocation experiments involving other nanoobjects.<sup>42</sup> Hereby, AuNP<sub>Arg3</sub> move faster than AuNP<sub>Arg9</sub>. This difference could be due to the charge differences between these two NPs. Indeed, when a NP has to cross a lipid bilayer, it has to overcome three energy barriers: a first hydrophilic energy barrier, which is

created by the hydrophilic heads; a second energy barrier that corresponds to the hydrophobic lipid tails; and finally, a third hydrophilic energy barrier, again due to the hydrophilic heads (see ref.<sup>27,30</sup>). Another explanation might be related to the higher rate of self-aggregation of AuNP<sub>Arg9</sub> on the lipid layer compared to AuNP<sub>Arg3</sub> due to highly positively charge surface of AuNP<sub>Arg9</sub> that can strongly interact to the negatively charge artificial membrane. These measured transport rates also depend on the bilayer composition. Until now, the bilayer composition was DOPC:DOPE (2:1) in total molar ratio.

We modify the lipid bilayer composition to see how the lipid packing is affecting the AuNP translocation. Moving the bilayer composition to 1:2 DOPC/DOPE, we find that the permeability of AuNP increases to  $P \approx 2.3 \mu\text{m}/\text{s}$  for AuNP<sub>Arg3</sub> and  $P \approx 2.1 \mu\text{m}/\text{s}$  for AuNP<sub>Arg9</sub>. This can be easily understood as DOPE lipids reduce the bilayer packing and increase the number of defects inside the bilayer, which facilitates the AuNPs translocation.<sup>43,44</sup> Furthermore, adding 10% DOPS (in total molar ratio) to this bilayer composition reduces the permeability of AuNP to  $P \approx 1.5 \mu\text{m}/\text{s}$  for AuNP<sub>Arg3</sub> and  $P \approx 1.3 \mu\text{m}/\text{s}$  for AuNP<sub>Arg9</sub>. DOPS lipids are negatively charged, which attracts the AuNPs, which are positively charged.<sup>45</sup> Therefore, it increases the value of the hydrophilic energy barrier produced by the hydrophilic head. It appears that this interaction raises the potential barrier that the AuNPs must overcome in order to travel across the bilayer. This effect is stronger for AuNP<sub>Arg9</sub> than for AuNP<sub>Arg3</sub>, as expected given AuNP<sub>Arg9</sub>'s higher positive charge. Along the same line, we did not measure any spontaneous transport of negatively charged AuNPs. This finding is not very surprising if we look at the negative zeta potential of DOPC liposomes.<sup>46</sup>

The experiments were repeated, but this time the DIB chamber's temperature is changed. Using an Arrhenius plot, we calculate the energetics of AuNPs translocation by plotting the permeability  $\ln(P)$  versus  $1/T$ , where  $T$  is the temperature in Kelvin (see Fig. 3).<sup>35</sup> The slope of this curve appears to be equal to  $E_a/R$ , where  $E_a$  is the activation energy and  $R$  is the gas constant. The extracted activation energies are shown in Figure 3, and their values are in the typical range of  $3 - 10 k_B T$ . The

extracted energy barriers are comparable to values reported in the literature.<sup>32,47</sup> As a result, the presence of DOPE reduced the potential barrier of a few  $k_B T$ . and the presence of DOPS increased the potential barrier of a few  $k_B T$ . Thus, AuNP<sub>Arg9</sub> has a faster translocation dynamic than AuNP<sub>Arg3</sub>.

## Conclusions

In this study, we report a quantitative and robust method to measure the collective translocation of gold nanoparticles across a droplet interface bilayer via dark-field microscopy. This method makes it easy and affordable to monitor the movement of unlabeled metallic nanoparticles over time. We investigate the efficiency and speed of translocation of ultra-small AuNPs (1.5 nm) with a tunable positively charged surface across an artificial lipid membrane mimicking a cell membrane. Transport is facilitated when the bilayer packing is reduced and hindered when the bilayer contains negatively charged lipids. This technique also allows the measurement of the activation energy barrier that particles must cross in order to pass through the bilayer. The associated energy barriers are reduced when the bilayer packing is reduced and increased when the bilayer contains negatively charged lipids. The extraction of these energy barriers is crucial since numerical forecasts rely on such challenging calculations of these barriers. The method described here can be easily adapted to measure the transfection of metal-containing nanoparticles with other designs and functional groups to better understand and handle the translocation of NP through the membrane in the context of drug delivery for biomedical applications.

## Materials and methods

### Molecules

1,2-dioleoyl-sn-glycero-3-phosphocholine (DOPC), 1,2-dioleoyl-sn-glycero-3-phosphoethanolamine (DOPE), 1,2-dioleoyl-sn-glycero-3-phosphoethanolamine-N-(7-nitro-2-1,3-benzoxadiazol-

4-yl) (NBD-DOPE) and 1,2-dioleoyl-sn-glycero-3-phospho-L-serine (DOPS) were purchased from Avanti Polar Lipids. For the microfluidic device preparation, the silicone elastomer Kit Sylgard 184 (PDMS) was purchased from Dow Corning. Ultra-pure water was obtained from an ultrapure filtration system (Thermo Fisher). All other chemicals, like sodium chloride, were purchased from Sigma-Aldrich. For the preparation of diluted protein solutions, phosphate buffer saline (PBS) was used. For the experiments, the buffer composition was always made of 150 mM KCl (Potassium chloride).

## AuNPs synthesis

All chemical products were bought from Sigma-aldrich (France) including the tripeptide Glutathione SG except for the peptide Arg3 (Cys-Arg-Arg; 589.76 g/mol), Arg9 (Cys-Arg Arg-Arg-Arg-Arg-Arg-Arg-Arg-Arg; 1526.97 g/mol) prepared in GenScript (Netherlands) with high purity ( $> 95\%$ ). Syntheses were performed using deionised water. Ultra-small gold nanoparticles AuNP<sub>Arg3</sub> stabilized by 25%vol Glutathione (SG) and 75%vol Arg3 was synthesized using a molar ratio Au/ Ligand/ NaBH<sub>4</sub> = 1/2/0.0125. Briefly, Arg3 and SG were mixed in 3mL of water and 96 $\mu$ L of HAuCl<sub>4</sub> sol (20mM) was added under rapid stirring at 500rpm. pH is then adjusted at 9 with NaOH (1M) and freshly prepared reducing agent NaBH<sub>4</sub> (1mM; 24 $\mu$ L) was added dropwise and kept stirred for 30min. Then, the pH is lowered down to 2 by adding HCl (1M) and the sol is kept under stirring for another 4 hours at 350rpm. Following this, the sol is precipitated in a mixture water/ethanol (30/70) and washed 3 times with a 3kDa Amicon filter to remove the unreactive products. The sol AuNP<sub>Arg3</sub> was then lyophilized for storage. The sol AuNP<sub>Arg9</sub> was prepared with similar protocol as AuNP<sub>Arg3</sub>. AuNPSG was prepared as described elsewhere.<sup>34</sup>

## Droplet Interface Bilayer Fabrication

To form droplet interface bilayer (DIBs), 2 mg/mL of lipids are dissolved into the oily phase (here squalene).<sup>48</sup> An oil-lipid mixture (here squalene) was filled into a hy-

drophobic (octadecyl-trichlorosilane, OTS-coated) cylindrical glass container with 7 cm diameter and a height of 1 cm. All the experiments were performed in a room with a controlled temperature using an homemade temperature control chamber. Transmission was used to look at a large part of the DiB with a Leica DM2700 microscope connected to a Leica color camera (MC170 HD). To form and manipulate aqueous microdroplets, micropipettes with a typical tip diameter in the range of 1 mm were formed using a micropipette puller. By injecting buffer solution (one with AuNPs, and one without) through two of these pipettes that were dipped in squalene, two droplets of almost the same size were made in this container. During this resting time, the lipids contained in the oil diffuse to the buffer/oil interface until decorate it. After about 30 min, the droplets were gently brought into contact with a needle. A few minutes after contacting the droplets, a lipid bilayer appears at the contact area between the droplets.<sup>4</sup> If not mentioned, the experiments were done at 23°C.

A mix of DOPC, DOPE, and DOPS is used to make the lipid bilayer composition that is used. DOPC/DOPE bilayer compositions with a 2:1 or 1:2 molar ratio and the same with 10% PS in total molar ratio are the tested bilayer compositions. Interestingly, the tension of such bilayers could be measured (as explained in ref<sup>35</sup>) and it is expressed in Figure 3. It appears that the bilayer tensions are similar for these tested lipid compositions. Pure DOPC bilayers and pure DOPE bilayers, were unstable for the required experiment lifetime.

## Author Contributions

J.-B.F performed and analyzed the DiBs experiments. S.M prepared the Au NPs. J-B F, V.F and X.LG discussed the data and wrote the manuscript. J.-B.F and X.LG directed the research.

## Conflicts of interest

The authors have no conflicts to declare.

## Acknowledgements

J.-B.F acknowledge funding from the SFB1027 (B4). X.LG and V.F. would like to thank la ligue contre le cancer (R2204CC) and "Investissements d'avenir" program (ANR-17-EURE-0003) for the financial support.

## References

- (1) Yeh, Y.-C.; Creran, B.; Rotello, V. M. Gold Nanoparticles: Preparation, Properties, and Applications in Bionanotechnology. Nanoscale **2012**, 4, 1871–1880.
- (2) Hammami, I.; Alabdallah, N. M.; jomaa, A. A.; kamoun, M. Gold nanoparticles: Synthesis properties and applications. Journal of King Saud University - Science **2021**, 33, 101560.
- (3) Yang, R.; Wei, T.; Goldberg, H.; Wang, W.; Cullion, K.; Kohane, D. S. Getting Drugs Across Biological Barriers. Advanced Materials **2017**, 29, 1606596, eprint: <https://onlinelibrary.wiley.com/doi/pdf/10.1002/adma.201606596>.
- (4) Bayley, H.; Cronin, B.; Heron, A.; Holden, M. A.; Hwang, W.; Syeda, R.; Thompson, J.; Wallace, M. Droplet interface bilayers. Mol Biosyst **2008**, 4, 1191–1208.
- (5) Huang, Y.; Fuller, G. G.; Chandran Suja, V. Physicochemical characteristics of droplet interface bilayers. Advances in Colloid and Interface Science **2022**, 304, 102666.
- (6) Fleury, J.-B.; A. Baulin, V.; Guével, X. L. Protein-coated nanoparticles exhibit Lévy flights on a suspended lipid bilayer. Nanoscale **2022**, 14, 13178–13186, Publisher: Royal Society of Chemistry.

- (7) Fleury, J.-B.; Werner, M.; Guével, X. L.; Baulin, V. A. Protein corona modulates interaction of spiky nanoparticles with lipid bilayers. Journal of Colloid and Interface Science **2021**,
- (8) Hu, M.; Novo, C.; Funston, A.; Wang, H.; Staleva, H.; Zou, S.; Mulvaney, P.; Xia, Y.; Hartland, G. V. Dark-field microscopy studies of single metal nanoparticles: understanding the factors that influence the linewidth of the localized surface plasmon resonance. J Mater Chem **2008**, 18, 1949–1960.
- (9) Broekgaarden, M.; Bulin, A.-L.; Porret, E.; Musnier, B.; Chovelon, B.; Ravet, C.; Sancey, L.; Elleaume, H.; Hainaut, P.; Coll, J.-L.; Guével, X. L. Surface functionalization of gold nanoclusters with arginine: a trade-off between microtumor uptake and radiotherapy enhancement. Nanoscale **2020**, 12, 6959–6963, Publisher: The Royal Society of Chemistry.
- (10) Guével, X. L.; Palomares, F.; Torres, M. J.; Blanca, M.; Fernandez, T. D.; Mayorga, C. Nanoparticle size influences the proliferative responses of lymphocyte subpopulations. RSC Adv. **2015**, 5, 85305–85309, Publisher: The Royal Society of Chemistry.
- (11) Poon, W.; Kingston, B. R.; Ouyang, B.; Ngo, W.; Chan, W. C. W. A framework for designing delivery systems. Nat. Nanotechnol. **2020**, 15, 819–829, Number: 10 Publisher: Nature Publishing Group.
- (12) Yang, Y.; Zeng, W.; Huang, P.; Zeng, X.; Mei, L. Smart materials for drug delivery and cancer therapy. VIEW **2021**, 2, 20200042, \_eprint: <https://onlinelibrary.wiley.com/doi/pdf/10.1002/VIW.20200042>.
- (13) Hornos Carneiro, M. F.; Barbosa, F. Gold nanoparticles: A critical review of therapeutic applications and toxicological aspects. Journal of Toxicology and Environmental Health, Part B **2016**, 19, 129–148, Publisher: Taylor & Francis \_eprint: <https://doi.org/10.1080/10937404.2016.1168762>.

- (14) Loynachan, C. N.; Soleimany, A. P.; Dudani, J. S.; Lin, Y.; Najer, A.; Bekdemir, A.; Chen, Q.; Bhatia, S. N.; Stevens, M. M. Renal clearable catalytic gold nanoclusters for in vivo disease monitoring. Nat Nanotechnol **2019**, 14, 883–890.
- (15) Porret, E.; Sancey, L.; Martín-Serrano, A.; Montañez, M. I.; Seeman, R.; Yahia-Ammar, A.; Okuno, H.; Gomez, F.; Ariza, A.; Hildebrandt, N.; Fleury, J.-B.; Coll, J.-L.; Le Guével, X. Hydrophobicity of Gold Nanoclusters Influences Their Interactions with Biological Barriers. Chem. Mater. **2017**, 29, 7497–7506, Publisher: American Chemical Society.
- (16) Lei, Y.; Tang, L.; Xie, Y.; Xianyu, Y.; Zhang, L.; Wang, P.; Hamada, Y.; Jiang, K.; Zheng, W.; Jiang, X. Gold nanoclusters-assisted delivery of NGF siRNA for effective treatment of pancreatic cancer. Nat Commun **2017**, 8, 15130, Number: 1 Publisher: Nature Publishing Group.
- (17) Du, B.; Jiang, X.; Das, A.; Zhou, Q.; Yu, M.; Jin, R.; Zheng, J. Glomerular barrier behaves as an atomically precise bandpass filter in a sub-nanometre regime. Nat Nanotechnol **2017**, 12, 1096–1102.
- (18) Panzarini, E.; Mariano, S.; Carata, E.; Mura, F.; Rossi, M.; Dini, L. Intracellular Transport of Silver and Gold Nanoparticles and Biological Responses: An Update. International Journal of Molecular Sciences **2018**, 19, 1305, Number: 5 Publisher: Multidisciplinary Digital Publishing Institute.
- (19) Peckys, D. B.; de Jonge, N. Visualizing Gold Nanoparticle Uptake in Live Cells with Liquid Scanning Transmission Electron Microscopy. Nano Lett. **2011**, 11, 1733–1738, Publisher: American Chemical Society.
- (20) Mousavi, S. A.; Malerød, L.; Berg, T.; Kjekken, R. Clathrin-dependent endocytosis. Biochem J **2004**, 377, 1–16.

- (21) Doherty, G. J.; McMahon, H. T. Mechanisms of Endocytosis. Annual Review of Biochemistry **2009**, 78, 857–902, eprint: <https://doi.org/10.1146/annurev.biochem.78.081307.110540>.
- (22) Li, B.; Lane, L. A. Probing the biological obstacles of nanomedicine with gold nanoparticles. WIREs Nanomedicine and Nanobiotechnology **2019**, 11, e1542, eprint: <https://onlinelibrary.wiley.com/doi/pdf/10.1002/wnan.1542>.
- (23) Orsi, M.; Essex, J. W. Permeability of drugs and hormones through a lipid bilayer: insights from dual-resolution molecular dynamics. Soft Matter **2010**, 6, 3797–3808, Publisher: The Royal Society of Chemistry.
- (24) Van Lehn, R. C.; Atukorale, P. U.; Carney, R. P.; Yang, Y.-S.; Stellacci, F.; Irvine, D. J.; Alexander-Katz, A. Effect of Particle Diameter and Surface Composition on the Spontaneous Fusion of Monolayer-Protected Gold Nanoparticles with Lipid Bilayers. Nano Lett. **2013**, 13, 4060–4067, Publisher: American Chemical Society.
- (25) Rocha, E. L. d.; Caramori, G. F.; Rambo, C. R. Nanoparticle translocation through a lipid bilayer tuned by surface chemistry. Phys. Chem. Chem. Phys. **2013**, 15, 2282–2290, Publisher: The Royal Society of Chemistry.
- (26) Treuel, L.; Jiang, X.; Nienhaus, G. U. New views on cellular uptake and trafficking of manufactured nanoparticles. J R Soc Interface **2013**, 10, 20120939.
- (27) Werner, M.; Auth, T.; Beales, P. A.; Fleury, J. B.; Höök, F.; Kress, H.; Van Lehn, R. C.; Müller, M.; Petrov, E. P.; Sarkisov, L.; Sommer, J.-U.; Baulin, V. A. Nanomaterial interactions with biomembranes: Bridging the gap between soft matter models and biological context. Biointerphases **2018**, 13, 028501, Publisher: American Vacuum Society.
- (28) Akimov, S. A.; Volynsky, P. E.; Galimzyanov, T. R.; Kuzmin, P. I.; Pavlov, K. V.; Batishchev, O. V. Pore formation in lipid membrane I: Continuous reversible

- trajectory from intact bilayer through hydrophobic defect to transversal pore. Sci Rep **2017**, 7, 12152.
- (29) Van Lehn, R. C.; Ricci, M.; Silva, P. H. J.; Andreozzi, P.; Reguera, J.; Voitchovsky, K.; Stellacci, F.; Alexander-Katz, A. Lipid tail protrusions mediate the insertion of nanoparticles into model cell membranes. Nat Commun **2014**, 5, 4482, Number: 1 Publisher: Nature Publishing Group.
- (30) Su, C.-F.; Merlitz, H.; Rabbel, H.; Sommer, J.-U. Nanoparticles of Various Degrees of Hydrophobicity Interacting with Lipid Membranes. J Phys Chem Lett **2017**, 8, 4069–4076.
- (31) Jackson, A. M.; Myerson, J. W.; Stellacci, F. Spontaneous assembly of subnanometre-ordered domains in the ligand shell of monolayer-protected nanoparticles. Nature Mater **2004**, 3, 330–336, Number: 5 Publisher: Nature Publishing Group.
- (32) Guo, Y.; Terazzi, E.; Seemann, R.; Fleury, J. B.; Baulin, V. A. Direct proof of spontaneous translocation of lipid-covered hydrophobic nanoparticles through a phospholipid bilayer. Science Advances **2016**, 2, e1600261, Publisher: American Association for the Advancement of Science Section: Research Article.
- (33) Er-Rafik, M.; Ferji, K.; Combet, J.; Sandre, O.; Lecommandoux, S.; Schmutz, M.; Meins, J.-F. L.; Marques, C. Tear of lipid membranes by nanoparticles. Soft Matter **2022**, 18, 3318–3322, Publisher: Royal Society of Chemistry.
- (34) Porret, E.; Jourdan, M.; Gennaro, B.; Comby-Zerbino, C.; Bertorelle, F.; Trouillet, V.; Qiu, X.; Zoukimian, C.; Boturyn, D.; Hildebrandt, N.; Antoine, R.; Coll, J.-L.; Le Guével, X. Influence of the Spatial Conformation of Charged Ligands on the Optical Properties of Gold Nanoclusters. J. Phys. Chem. C **2019**, 123, 26705–26717, Publisher: American Chemical Society.
- (35) Fleury, J.-B. Enhanced water permeability across a physiological droplet interface

- bilayer doped with fullerenes. RSC Adv. **2020**, 10, 19686–19692, Publisher: The Royal Society of Chemistry.
- (36) Weigel, A.; Sebesta, A.; Kukura, P. Dark Field Microspectroscopy with Single Molecule Fluorescence Sensitivity. ACS Photonics **2014**, 1, 848–856, Publisher: American Chemical Society.
- (37) Faugeras, V.; Duclos, O.; Bazile, D.; Thiam, A. R. Membrane determinants for the passive translocation of analytes through droplet interface bilayers. Soft Matter **2020**, 16, 5970–5980, Publisher: The Royal Society of Chemistry.
- (38) Milianta, P. J.; Muzzio, M.; Denver, J.; Cawley, G.; Lee, S. Water Permeability across Symmetric and Asymmetric Droplet Interface Bilayers: Interaction of Cholesterol Sulfate with DPhPC. Langmuir **2015**, 31, 12187–12196, Publisher: American Chemical Society.
- (39) Katopodes, N. D. In Free-Surface Flow; Katopodes, N. D., Ed.; Butterworth-Heinemann, 2019; pp 184–270.
- (40) Allolio, C.; Magarkar, A.; Jurkiewicz, P.; Baxová, K.; Javanainen, M.; Mason, P. E.; Šachl, R.; Cebecauer, M.; Hof, M.; Horinek, D.; Heinz, V.; Rachel, R.; Ziegler, C. M.; Schröfel, A.; Jungwirth, P. Arginine-rich cell-penetrating peptides induce membrane multilamellarity and subsequently enter via formation of a fusion pore. Proceedings of the National Academy of Sciences **2018**, 115, 11923–11928, Publisher: Proceedings of the National Academy of Sciences.
- (41) Wright, L. B.; Merrill, N. A.; Knecht, M. R.; Walsh, T. R. Structure of arginine overlayers at the aqueous gold interface: implications for nanoparticle assembly. ACS Appl Mater Interfaces **2014**, 6, 10524–10533.
- (42) Faugeras, V.; Duclos, O.; Bazile, D.; Thiam, A. R. Impact of Cyclization and Methylation on Peptide Penetration through Droplet Interface Bilayers. Langmuir **2022**, 38, 5682–5691, Publisher: American Chemical Society.

- (43) Asfia, S.; Seemann, R.; Fleury, J.-B. Phospholipids diffusion on the surface of model lipid droplets. Biochimica et Biophysica Acta (BBA) - Biomembranes **2023**, 1865, 184074.
- (44) Sikdar, S.; Rani, G.; Vemparala, S. Role of lipid packing defects in determining membrane interactions of antimicrobial polymers. 2022; <https://www.biorxiv.org/content/10.1101/2022.06.08.495334v1>, Pages: 2022.06.08.495334 Section: New Results.
- (45) Pöyry, S.; Vattulainen, I. Role of charged lipids in membrane structures — Insight given by simulations. Biochimica et Biophysica Acta (BBA) - Biomembranes **2016**, 1858, 2322–2333.
- (46) Chibowski, E.; Szcześ, A. Zeta potential and surface charge of DPPC and DOPC liposomes in the presence of PLC enzyme. Adsorption **2016**, 22, 755–765.
- (47) Burgess, S.; Wang, Z.; Vishnyakov, A.; Neimark, A. V. Adhesion, intake, and release of nanoparticles by lipid bilayers. Journal of Colloid and Interface Science **2020**, 561, 58–70.
- (48) Heo, P.; Ramakrishnan, S.; Coleman, J.; Rothman, J. E.; Fleury, J.-B.; Pincet, F. Highly Reproducible Physiological Asymmetric Membrane with Freely Diffusing Embedded Proteins in a 3D-Printed Microfluidic Setup. Small **2019**, 15, 1900725, .eprint: <https://onlinelibrary.wiley.com/doi/pdf/10.1002/sml.201900725>.